Supplementary Material for

J. Rachel Carr[1], Emily A. Hill[2], and G. Hilmar Gudmundsson[2]

[1]School of Geography, Politics, and Sociology, Newcastle University, Newcastle-upon-Tyne, NE1 7RU, UK
[2]Department of Geography and Environmental Sciences, Northumbria University, Newcastle-upon-Tyne, NE1 8ST, UK

**Correspondence:** Rachel Carr (rachel.carr@newcastle.ac.uk)

Text

Table S1. Mean errors and misfits between observed and modelled velocities for different multiples of dhdt errors (m a^{-1}) at Humboldt Gletsjer

|	No dhdt	dhdt error*1	dhdt error*2	dhdt error*5	dhdt error*10
Velocity misfit (m a^{-1})	8.085	129.903	64.868	28.956	16.949
Mean velocity error (m a^{-1})	N/A	0.047	0.094	0.235	0.047

Table S2. Modelled and measured flux in m a^{-1} for Kangerdluggsuaq Gletsjer (KG), Humboldt Gletsjer (HG) and Petermann Gletsjer (PG), for each sliding law. Measured fluxes are sourced from Mouginot et al (2019) for the year 2014 and the average flux for 2010-2018. These are compared to the modelled flux at the start of the forward run experiments, i.e. at the start of 2015, as ice velocities from winter 2014/15 were used to initialise the model.

| Glacier	Weertman (W)	Budd (W-N0)	Tsai (minCW-N0)	Cornford (rCW-N0)	Measured (2014)	Measured (2010-18)
KG	25.91	26.12	25.90	25.92	26.2± 5.6	26.6± 5.6
HU	5.93	5.96	5.93	5.93	4.7 ± 1.2	4.9 ± 1.2
PG	12.09	12.09	12.09	12.09	11.2 ± 1.2	11.2 ± 1.2
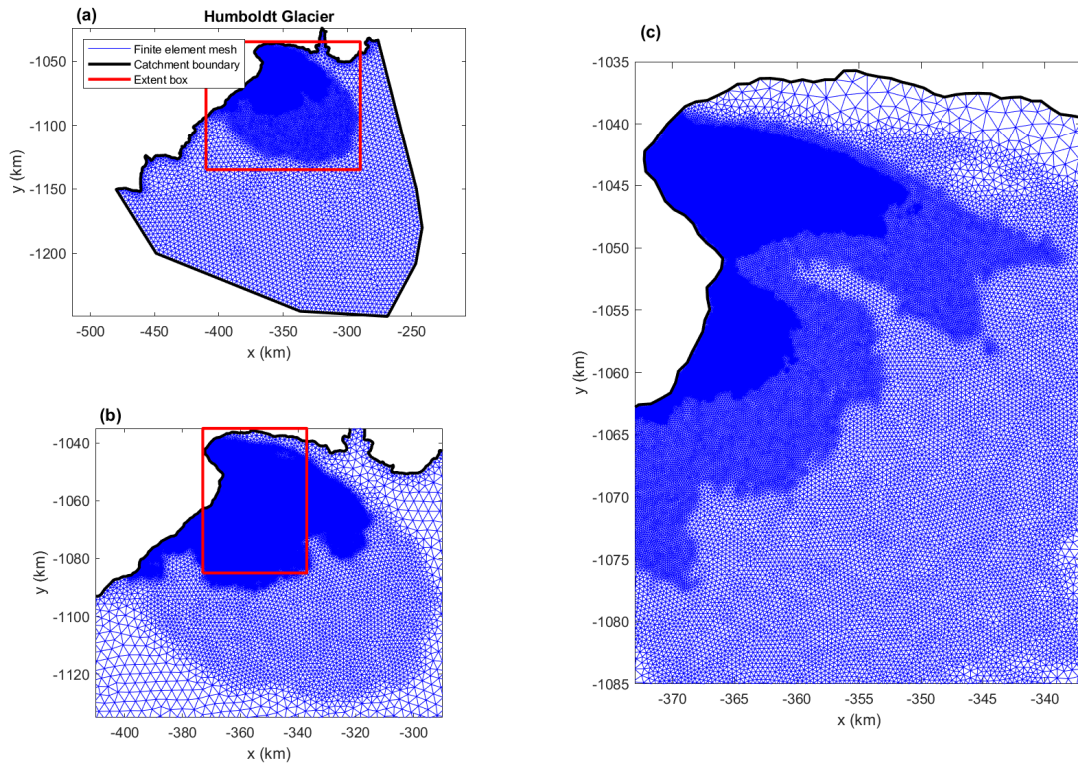
Figure S1. Finite element mesh for Humboldt Gletsjer (HU). The insets show the mesh at higher resolutions over the faster flowing areas. Element sizes are smallest in the areas of fastest flow, and larger towards the slower flowing inland regions of the glacier catchment. The element sizes are given in Table A1.
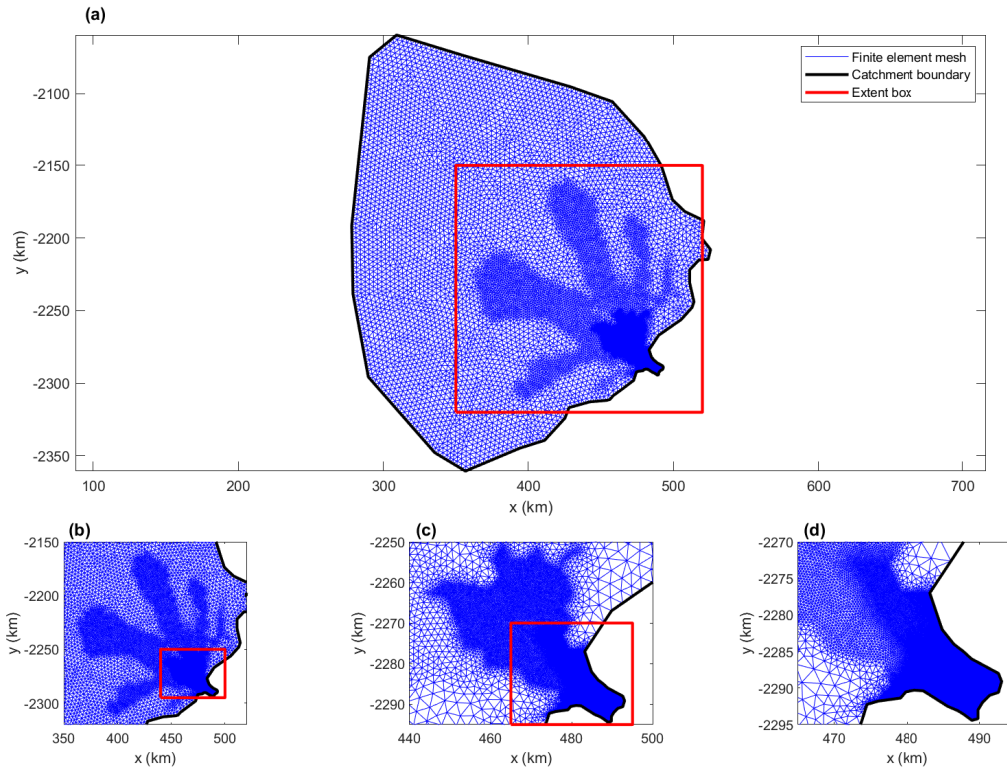
Figure S2. Finite element mesh for Kangerdluggsuaq Gletsjer (KG). The insets show the mesh at higher resolutions over the faster flowing areas. Element sizes are smallest in the areas of fastest flow, and larger towards the slower flowing inland regions of the glacier catchment. The element sizes are given in Table A1.
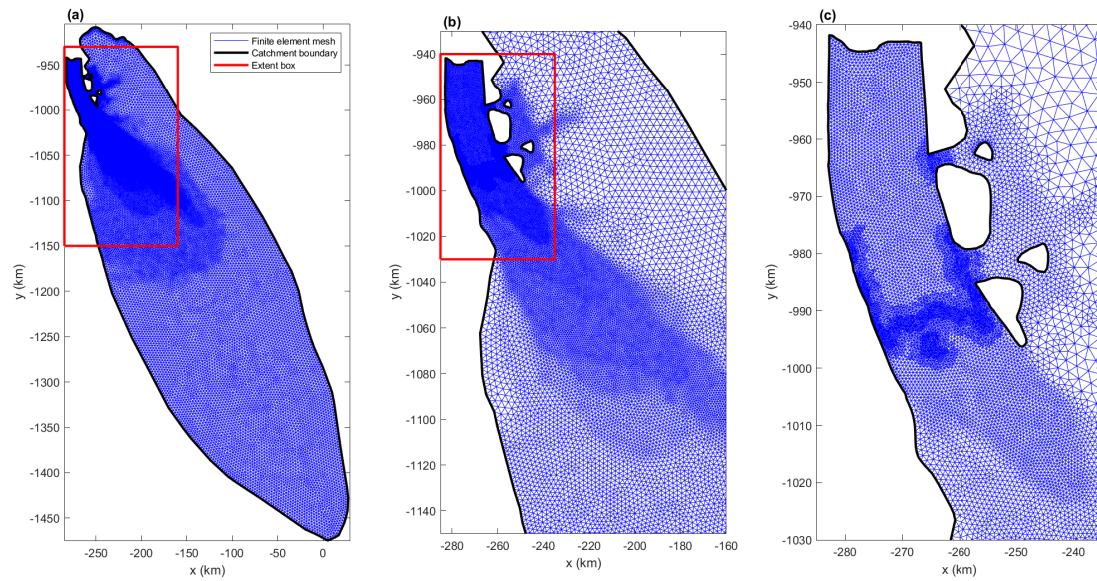
Figure S3. Finite element mesh for Petermann Gletsjer (PG). The insets show the mesh at higher resolutions over the faster flowing areas. Element sizes are smallest in the areas of fastest flow, and larger towards the slower flowing inland regions of the glacier catchment. The element sizes are given in Table A1.
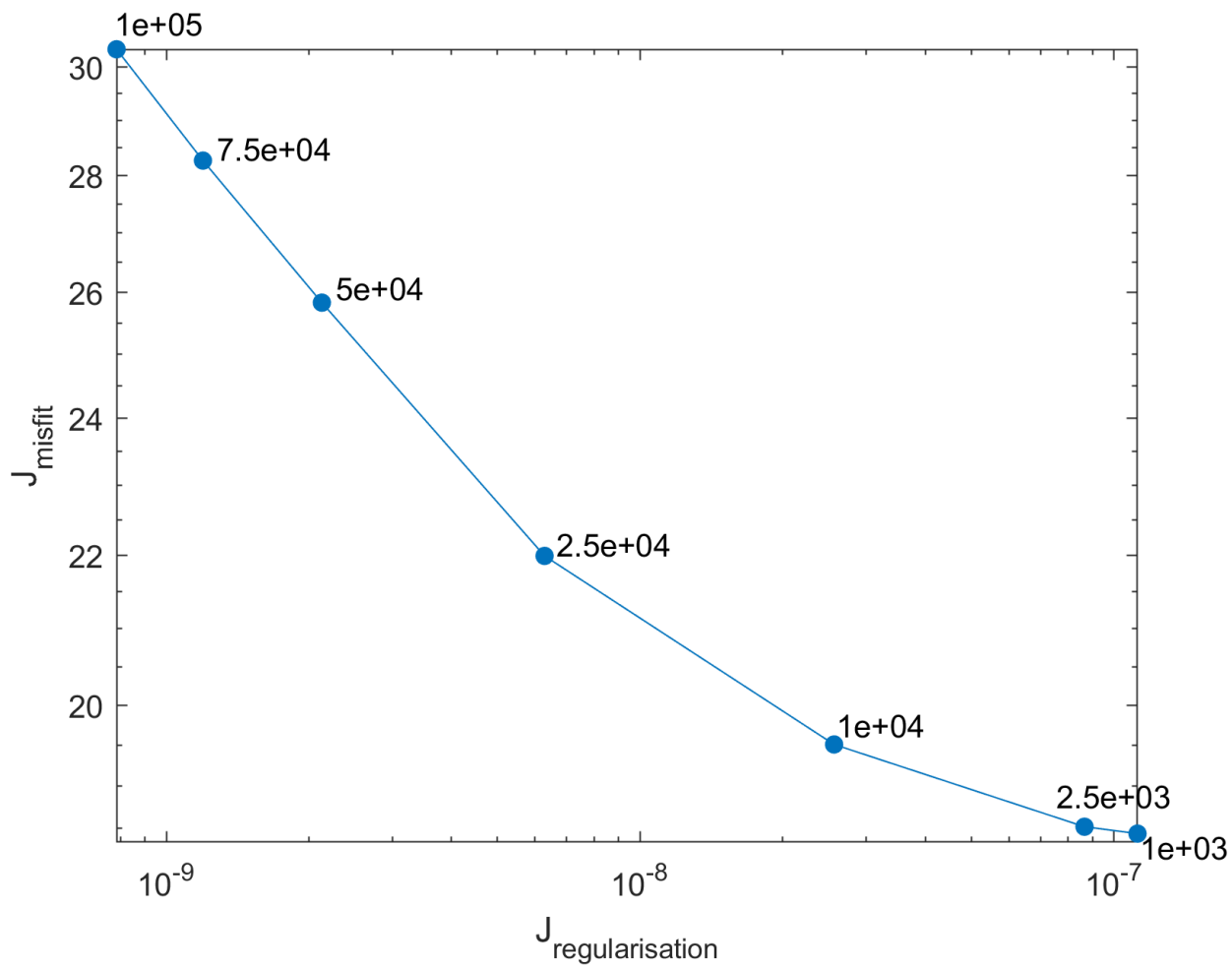
**Figure S4.** Example $L-$curve
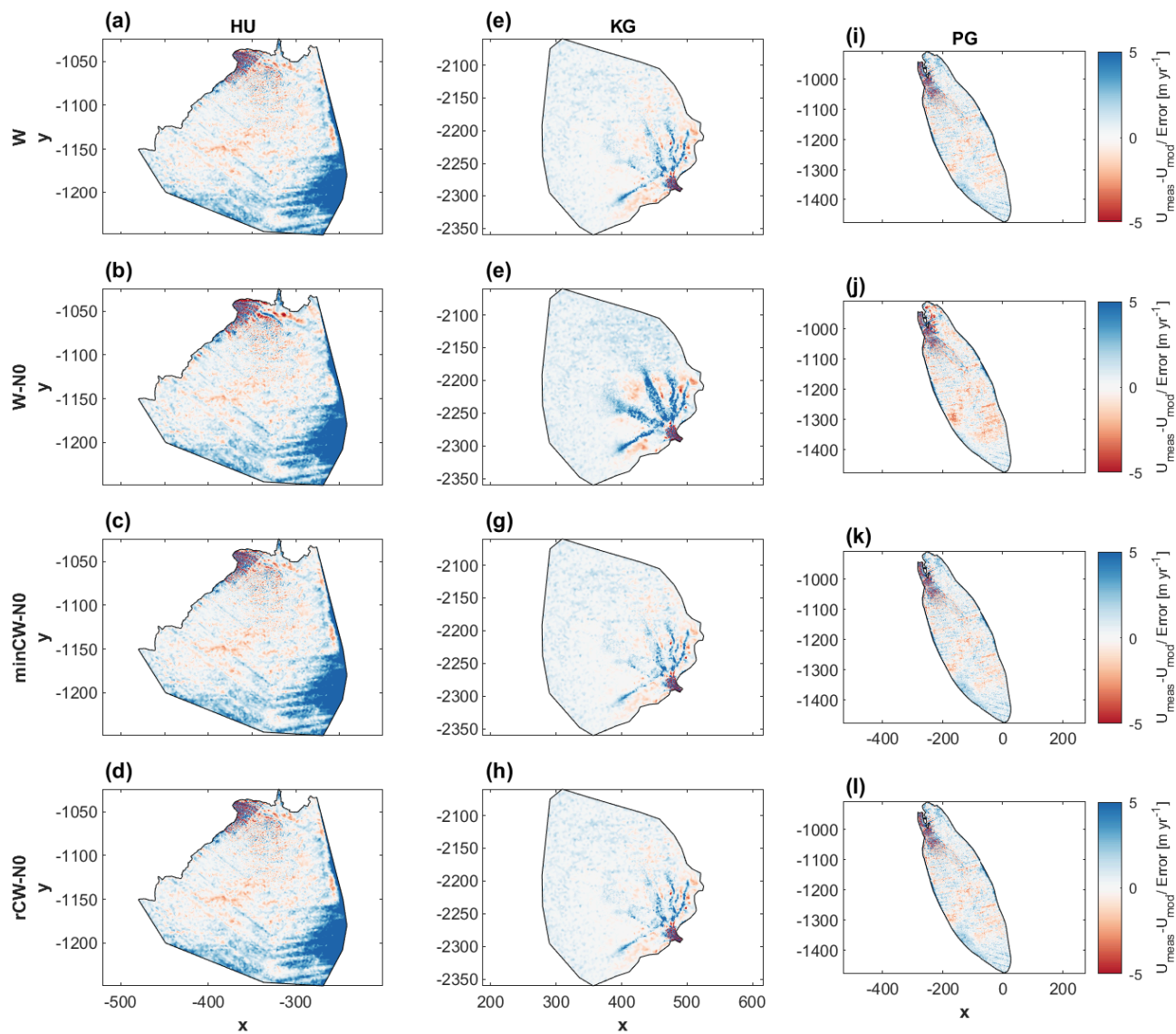
Figure S5. Velocity misfits at the end of the inversion for Kangerlugssuaq Gletsjer (left column:a-d) Humboldt Gletsjer (middle column:e-h) and Petermann Gletsjer (right column:i-l), using the Weertman (first row), Budd (second row), Tsai (third row) and Cornford (fourth row) sliding laws. The data show measured speed minus modelled speed, divided by the error.
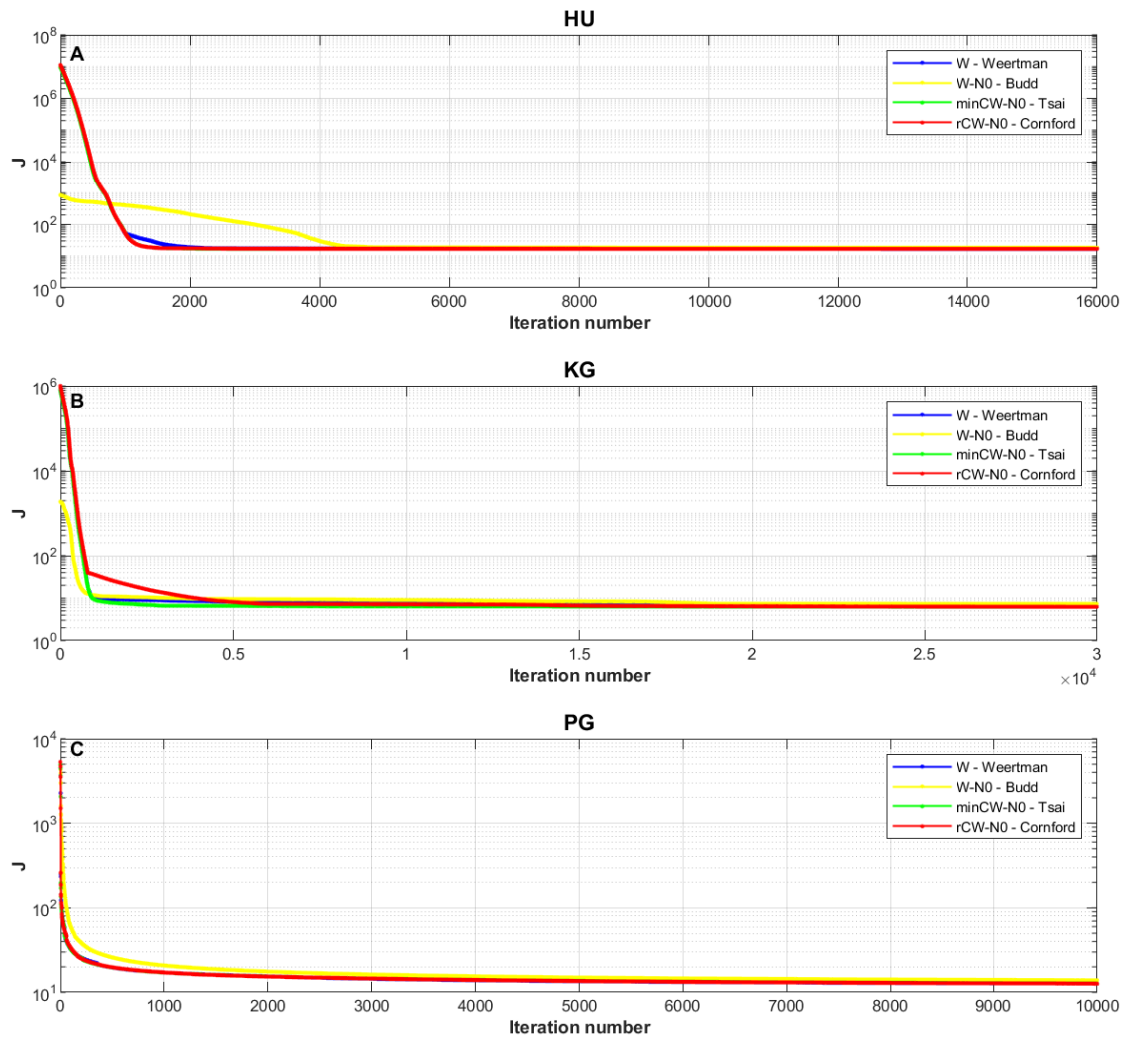
Figure S6. Inversion optimisation for A) Humboldt Gletsjer (HU), B) Kangerdlugssuaq Gletsjer (KG) and C) Petermann Gletsjer (PG), for each sliding law.
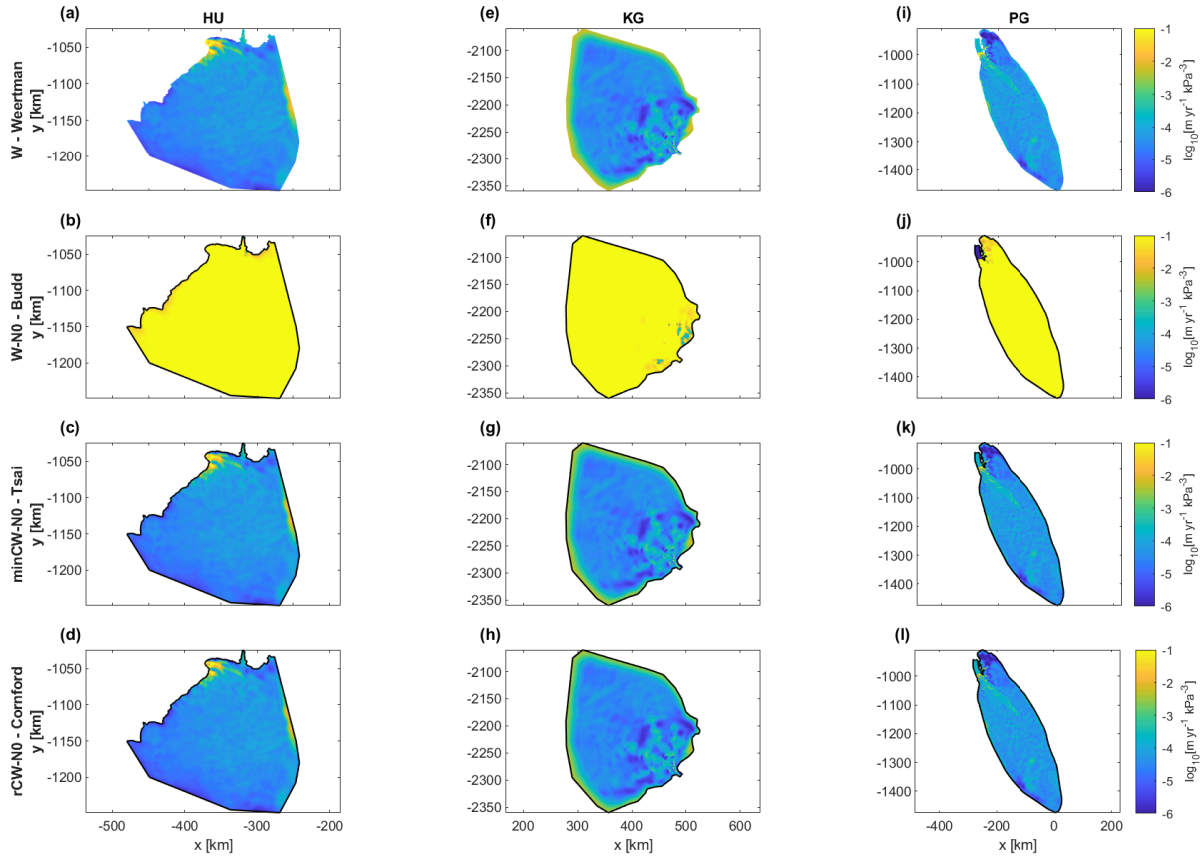
Figure S7. C fields at the end of the inversion for Humboldt Gletsjer (HU; left column) Kangerlugssuaq Gletsjer (KG; middle column) and Petermann Gletsjer (PG; right column), using the Weertman (first row), Budd (second row), Tsai (third row) and Cornford (fourth row) sliding laws.
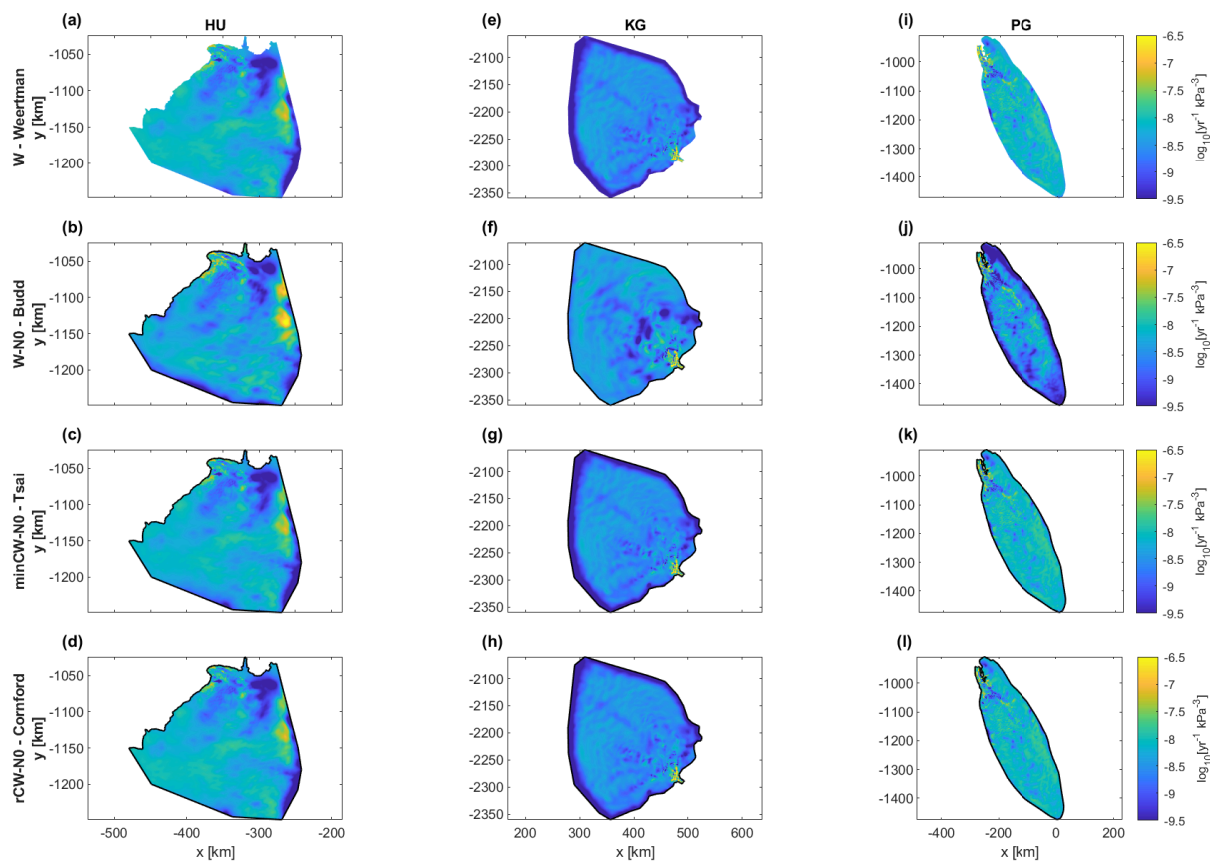
Figure S8. A Glen fields at the end of the inversion for Humboldt Gletsjer (HU; left column) Kangerlugssuaq Gletsjer (KG; middle column) and Petermann Gletsjer (PG; right column), using the Weertman (first row), Budd (second row), Tsai (third row) and Cornford (fourth row) sliding laws
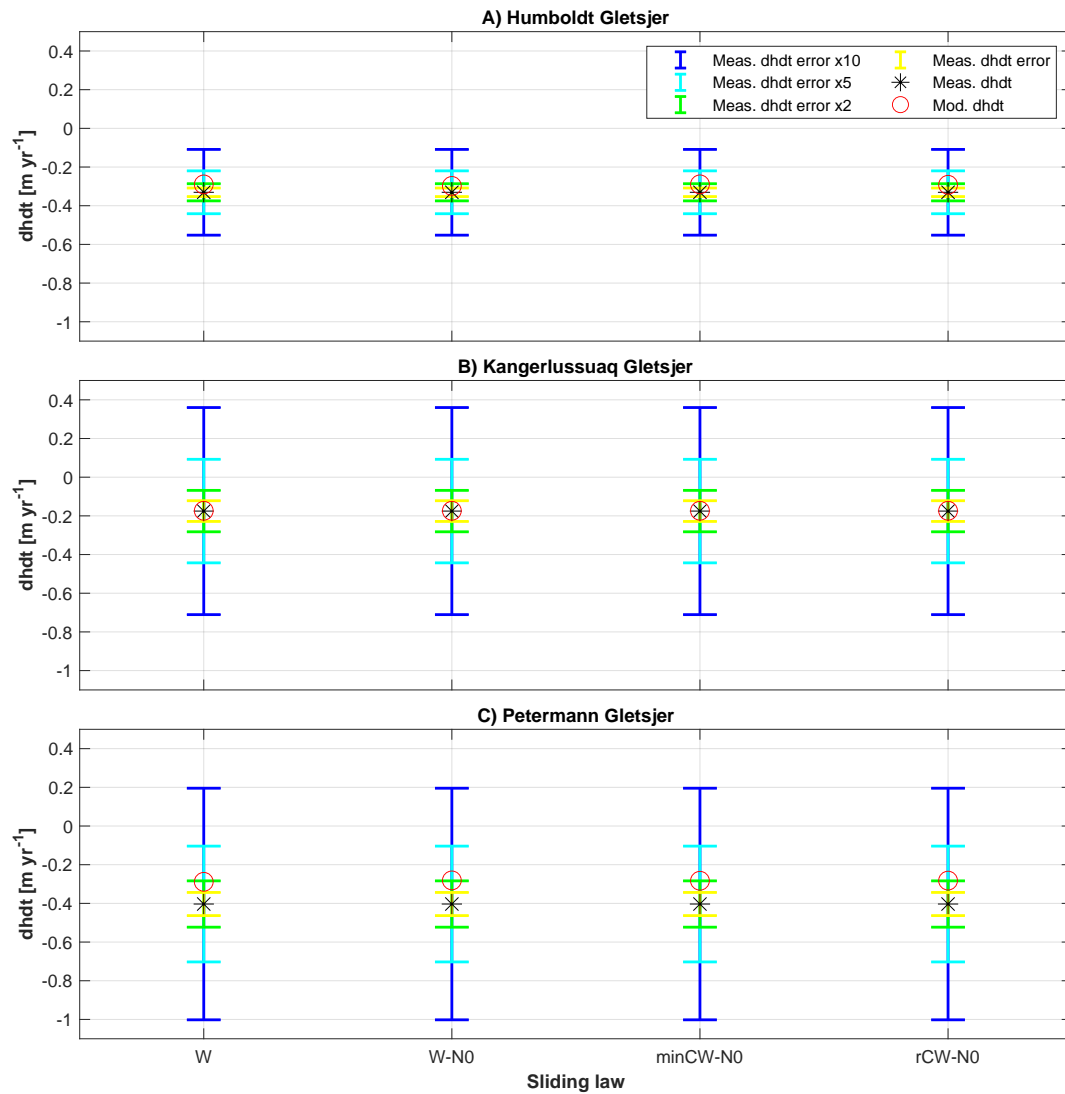
Figure S9. Integrated modelled and measured dhdt at 2015, following the 5 year dhdt adjutstment period for: A) Humboldt Gletsjer; B) Kangerlugssuaq Gletsjer; and C) Petermann Gletsjer. For each glacier, measured dhdt (black asterisk) and modelled dhdt (red circle) in 2015 are shown. Values were itnegrated across each glacier catchment, to give catchment-averaged measured and modelled dhdt values. Bars show the catchment-integrated error values provided with the measured dhdt data (yellow), the errors multiplied by 2 (green), by 5 (cyan) and by 10 (blue).

11
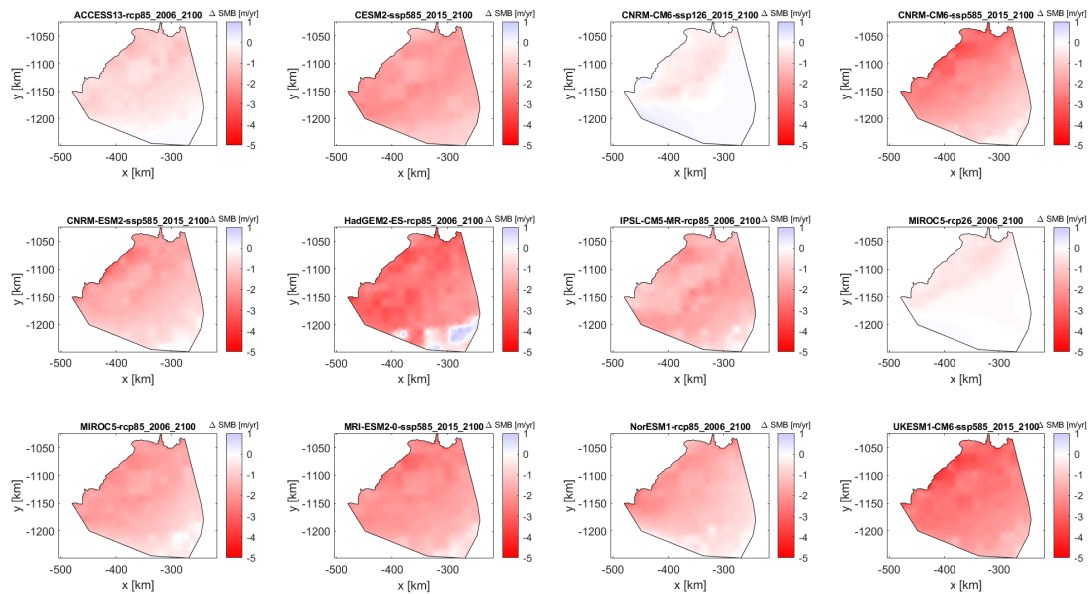
Figure S10. Forecast changes in surface mass balance (SMB) between 2015 and 2100 for Humboldt Gletsjer, according to SMB scenario. Red indicates negative SMB and blue indicates positive SMB. Subplots are order alphabetically, according to scenario name.
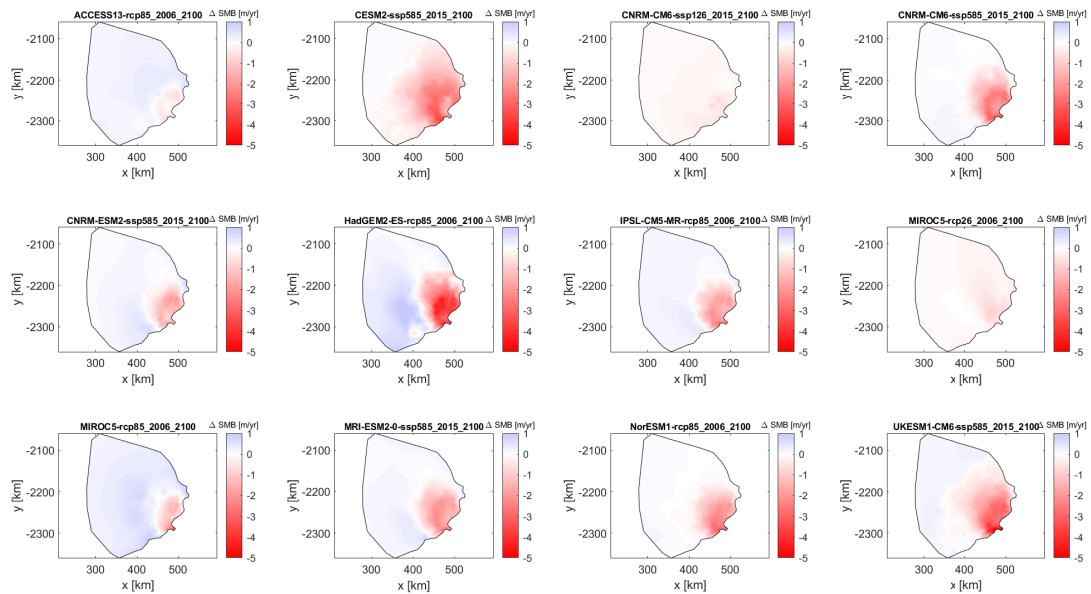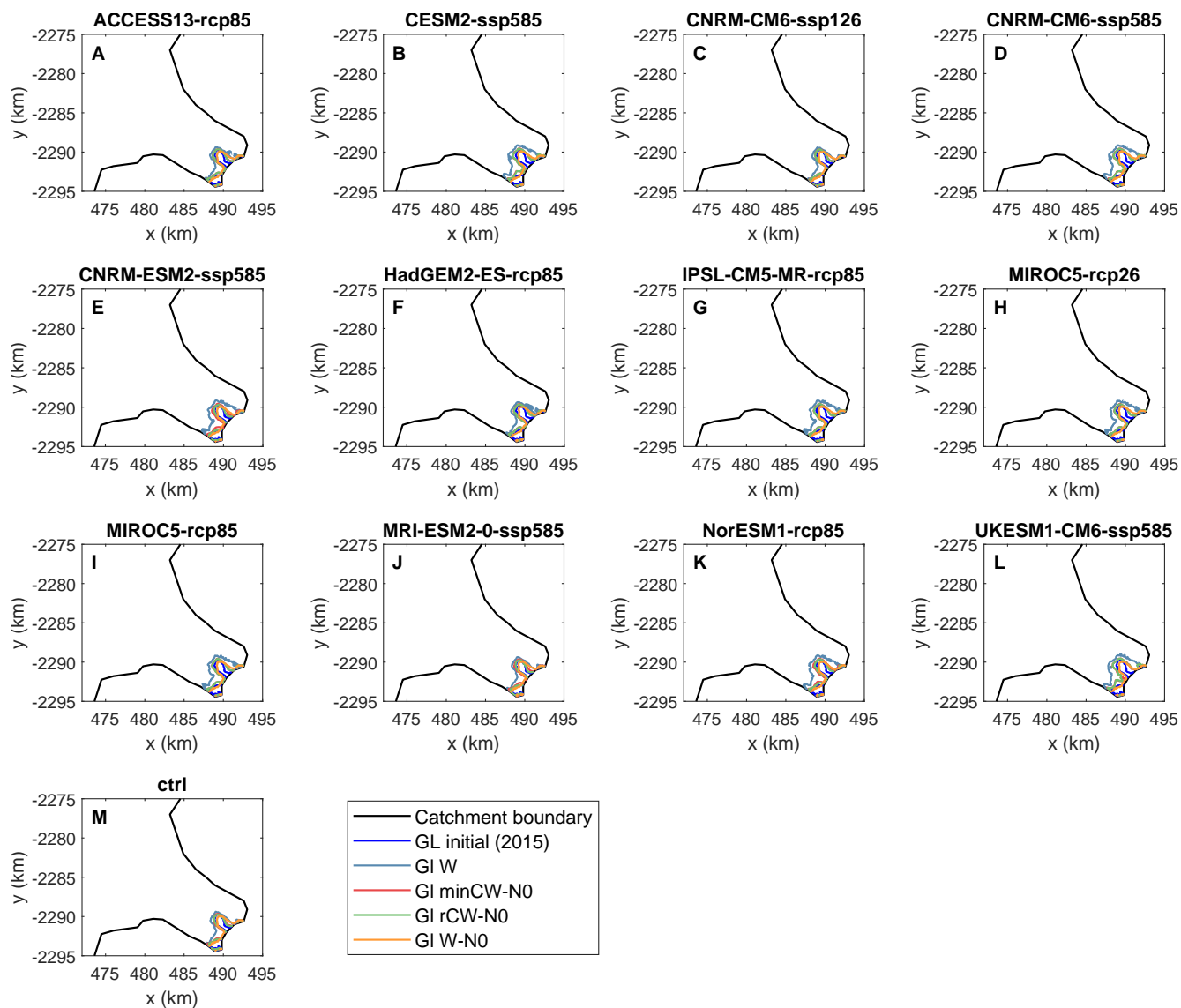
Figure S11. Forecast changes in surface mass balance (SMB) between 2015 and 2100 for Kangerdlugssuaq Gletsjer, according to SMB scenario. Red indicates negative SMB and blue indicates positive SMB. Subplots are order alphabetically, according to scenario name.

13
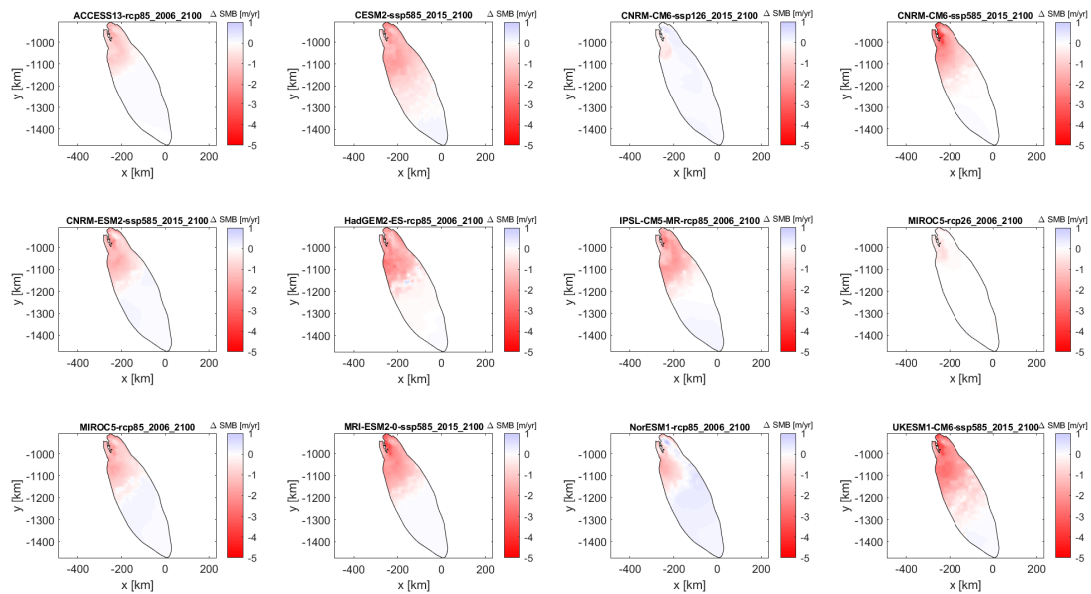
Figure S12. Forecast changes in surface mass balance (SMB) between 2015 and 2100 for Petermann Gletsjer, according to SMB scenario. Red indicates negative SMB and blue indicates positive SMB. Subplots are order alphabetically, according to scenario name.
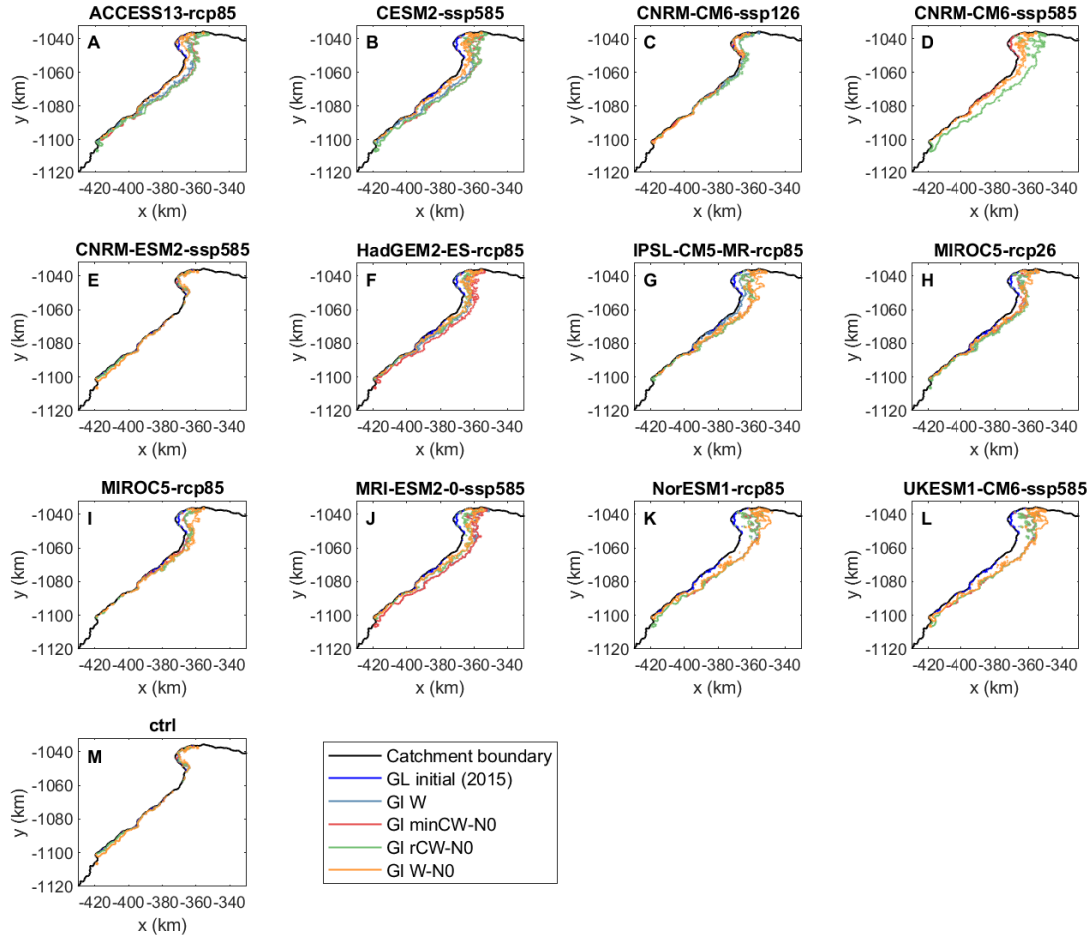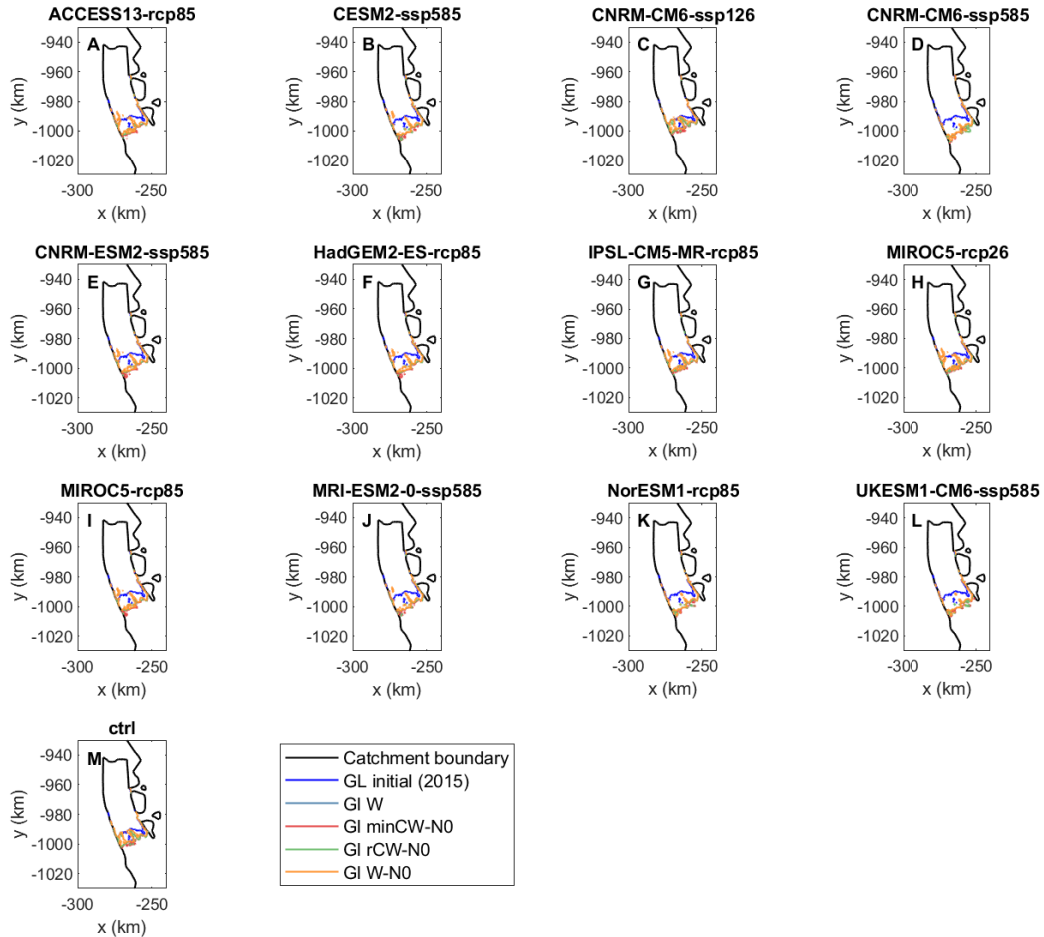
Figure S13. Changes in grounding line position between 2015 and 2100 for Humboldt Gletsjer (HU), according sliding law and surface mass balance forecast (SMB). Plots are divided by SMB forecast, given in the subplot title. The results are coloured-coded by sliding law: minCW-N0 = Tsai; rCW-N0 = Cornford; W = Weertman; and W-N0 = Budd.

Figure S14. Changes in grounding line position between 2015 and 2100 for Kangerluggsuaq Gletsjer (KG), according sliding law and surface mass balance forecast (SMB). Plots are divided by SMB forecast, given in the subplot title. The results are coloured-coded by sliding law: minCW-N0 = Tsai; rCW-N0 = Cornford; W = Weertman; and W-N0 = Budd.

Figure S15. Changes in grounding line position between 2015 and 2100 for Petermann Gletsjer (PG), according sliding law and surface mass balance forecast (SMB). Plots are divided by SMB forecast, given in the subplot title. The results are coloured-coded by sliding law: minCW-N0 = Tsai; rCW-N0 = Cornford; W = Weertman; and W-N0 = Budd.